Experimental Mechanics (2015) 55:1395–1409
DOI 10.1007/s11340-015-0035-z

Experimental Characterization of Unimorph Shape Memory Polymer Actuators Incorporating Transverse Curvature in the Substrate

J.T. Cantrell[1] · **P.G. Ifju**[1]

Received: 24 March 2014 / Accepted: 27 April 2015 / Published online: 9 June 2015

Abstract Shape memory polymers (SMP) have the potential to be utilized as a lightweight, solid state actuator in modern reconfigurable structures including as a deployment system for satellite solar panels or morphing aircraft wings. This paper is primarily concerned with the use of Veriflex-S® shape memory polymer and bi-directional carbon-fiber-reinforced-polymer (CFRP) in a flexural unimorph actuator configuration. One of the major deficiencies of SMP unimorphs is the permanent set (unrecovered shape) after a single or multiple temperature cycle(s). The novel concept of incorporating transverse curvature in the CFRP substrate, similar to that of an extendable tape measurer, is proposed to improve the shape recovery by increasing the bending stiffness of the unimorph actuator to compensate for the lack of recovery of the SMP. A set of experiments was designed to investigate the influence of transverse curvature, the relative widths of SMP and CFRP substrates, and shape memory polymer thickness on actuator recoverability after multiple thermo-mechanical cycles. The performance of SMP unimorph actuators with varying degrees of transverse curvature were evaluated versus that of traditional SMP unimorphs incorporating a flat substrate. Digital image correlation was implemented to quantify the out-of-plane deflection of the unimorph composite actuators (UCAs) during the actuation cycle. Experimental results indicate that an actuator with transverse curvature significantly reduces the residual deformation by at least two orders of magnitude which could be further tailored to enhance the performance of shape memory polymers in reconfigurable arrangements.

✉ J. T. Cantrell
jasontcantrell@gmail.com

[1] Department of Mechanical and Aerospace Engineering, University of Florida, Gainesville, FL 32611, USA

Keywords Shape memory polymer · Unimorph · Transverse curvature · Digital image correlation · Composites

Nomenclature

ρ	Substrate Radius of Curvature
c	Polymer Width
CF	Carbon Fiber
CFRP	Carbon-Fiber-Reinforced Polymer
CTE	Coefficient of Thermal Expansion
CV	Coefficient of Variation
DIC	Digital Image Correlation
L	Actuator Length
MAV	Micro Air Vehicle
s	Substrate Width
SMP	Shape Memory Polymer
t	Polymer Thickness
T_g	Glass Transition Temperature
UCA	Unimorph Composite Actuator
u,v,w	Lengthwise, Widthwise, and Vertical Displacements
x,y,z	Lengthwise, Widthwise, and Vertical Coordinates

Introduction

Shape memory polymers (SMPs) are a category of smart material with the ability to change their shape upon the application of external stimuli such as temperature [1–3], electricity [4–6], magnetism [7–9], or light [10–14]. Classes of smart materials include piezoelectrics, shape memory alloys, and shape memory polymers. Varieties of smart materials practical for various applications include shape memory alloys in orthodontic treatments, piezoelectric actuators for control of micro air vehicles, shape memory polymers as cardiovascular stents, and a multitude of smart materials for the morphing

of aircraft structures [15–24]. Veriflex-S®, the SMP provided by our sponsors for investigation in this paper, uses a thermal external stimulus to allow reconfiguration and recovery. Veriflex-S®, and Veriflex-E®, its higher glass transition temperature counterpart, have been studied extensively by researchers including Li et al. [2, 25–27], Fulcher, et al. [28–31], Nahid, et al.[32], McClung, et al. [33–38], Lu, et al. [39–42], Chowdhury et al. [43, 44], Liu, et al. [45], Cortes, et al. [46], Beblo et al. [47, 48], and Atli, et al. [49]. The Veriflex® SMPs have been utilized for notable applications including active disassembly for recycling, deployment of satellite solar panels, and deployable aircraft wings [22, 50, 51].

Veriflex® can be divided into two categories of stiffness and material behavior: the high glassy modulus and low rubbery modulus [35, 36]. At temperatures below the glass transition temperature (T_g) of 62 °C, Veriflex-S® is relatively stiff and has a high elastic modulus (~1 GPa); however, once the SMP is heated above T_g the modulus drops by several orders of magnitude (~1 MPa). Veriflex-S® can achieve strains of approximately 140 % while in the rubbery state and after cooling below T_g maintain this new deformed shape indefinitely [43, 44]. Other specialized SMPs are capable of strains up to 800 % in the rubbery state [52, 53]. The original/programmed shape can be recovered by heating the polymer above T_g again. The glassy state is classified as the temperatures lying 10 °C or more below the T_g, while the rubbery state is identified as temperatures lying 10 °C or greater above the T_g [54]. The area in between the glassy and rubbery state is classified as the transition region in which the elastic modulus transitions rapidly.

SMPs can change their shape from their original/programmed shape (flat beams in this study) to a deformed/stored shape and then return to a deployed shape (ideally the same as the original/programmed shape) when exposed to elevated temperatures. An illustration of an ideal shape memory thermo-mechanical cycle is shown in Fig. 1. The SMP begins in its original shape (Step 1) at a high modulus below T_g and then heat is applied to the sample causing the modulus to fall into the rubbery state (Step 2). Once in the rubbery state the sample is bent into the desired deformed shape (a U-shaped configuration for this study, Step 3) and then allowed to cool below T_g locking the current deformed shape (Step 4). The sample can be stored indefinitely in this unloaded configuration (Step 5) while awaiting the reapplication of heat. After heating, the sample will release and return to the unconstrained original/programmed form (Step 6). The sample is then cooled (Step 7) and would ideally return to 100 % of the original shape seen before the heating cycle. However, in reality, the Veriflex® SMP can achieve a final shape that is only close to the original shape (the deployed shape in this study). This is reiterated in Fig. 2 which explains the ideal versus actual stress–strain-temperature behavior for an SMP during a thermo-mechanical cycle. The idealized and actual cycles are identical until the load is released, the fifth step in the cycle. Ideally, the SMP locks into its current configuration, however in actuality there is some relaxation that occurs during this step. This is shown as shape retention or "fixity" loss in Fig. 2. Once reheated and cooled the shape memory will try to recover to its original/programmed shape. However, as the actual cycle shows the SMP is unable to recover fully and exhibits some degree of shape recovery loss. Various researchers have studied this behavior and determined that the recoverability of SMP can vary from as low as 65 % to nearly 100 % of the original shape depending upon testing conditions [35, 51, 55, 56].

Despite these hindrances SMPs are still advantageous over other shape memory materials due to the fact that they are low cost, low density, and highly deformable among other benefits [57, 58]. Shape memory materials are valued for their potential use in adaptive structures in applications such as micro air vehicles (MAVs) and morphing aircraft [59]. The University of Florida has worked with adaptive structures and MAVs extensively, adopting both active adaptation with piezoelectric actuators and passive adaptation with flexible membrane wings [16, 17, 60–64] . Ifju et al. developed a bendable load stiffened MAV wing that is compliant in the downward direction for storing the aircraft, but uses the wing curvature to avoid buckling due to flight loads [65–67]. Using this knowledge of MAVs and morphing wing structures, a plan of study was devised for a multipurpose morphing actuator to determine if the same bendable composite technology used in MAV wings could assist in increasing the recoverability of the Veriflex-S® SMP. In order to properly understand the overall performance of the SMP in a unimorph composite actuator (UCA) configuration, digital image correlation (DIC) testing was incorporated to determine the residual deformation present. A UCA was described as an element capable of bi-stable configuration when supplied with an external stimulus (heat in this case) consisting of one active layer (SMP) to which the stimulus is applied and one inactive layer (CFRP) that supports the active layer. A flat CFRP beam (designated as the CFRP, composite, or simply carbon fiber (CF) substrate throughout the paper) with SMP adhered to its surface was compared against a transversely curved CF beam with curvature similar to that of the MAV wing discussed previously. Additionally, a more detailed survey of the design space investigating the influence of other variables present was also documented via DIC. The details of the UCA analysis and the experimental procedure are explained in the subsequent sections. During the course of experimenting with flat flexural unimorph actuators, research indicated that by incorporating transverse curvature (similar to an extendable tape measure) in the CF layer one can vastly improve the shape recovery of an SMP unimorph actuator. The marked increase in recovery is attributed to the increased bending stiffness of

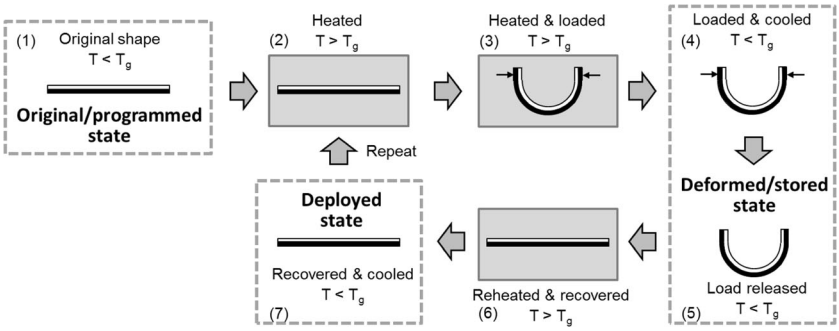

Fig. 1 Illustration of a shape memory cycle for the recovery of thermally activated SMPs. The shape memory polymer is originally programmed as a flat beam (*1*), heated above T_g (*2*), deformed into the desired configuration (*3*), cooled (*4*), released from loading (*5*), heated again (*6*), and finally allowed to recover to its deployed flat state while cooling (*7*)

the unimorph actuator such that it dominates the mechanical response of the SMP and improves the overall recoverability. The substrate functions in a bi-stable manner much like an extendable taper measurer, where it has high longitudinal bending stiffness while extended (straight) and relatively low stiffness when rolled. The transverse curvature provides the high longitudinal stiffness in the straight or near-straight configurations (original/programmed and deployed states). Once large longitudinal curvature is applied (deformed/stored state), the transverse curvature flattens and allows for the equivalent ease of deformation as that of an initially flat substrate. This can be seen in Fig. 3 where three versions of the UCAs are depicted in the stored configuration. Upon reheating the SMP and substrate proceed back towards the original/programmed state. However, the SMP does not completely recover. The substrate retains the transverse curvature and overpowers the SMPs poor recovery resulting in a significant reduction in overall residual deformation of the UCA. The subsequent sections will cover the findings from the investigation of flexural SMP unimorphs.

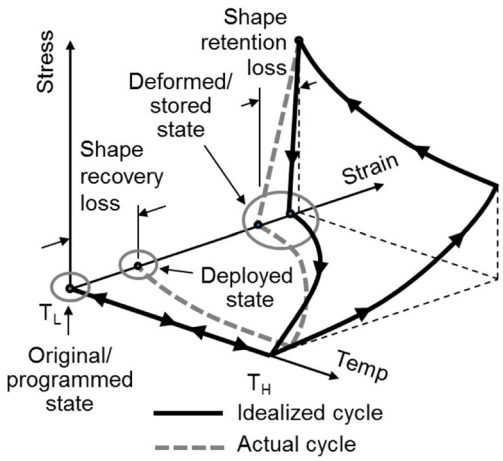

Fig. 2 Schematic of the stress–strain-temperature behavior of a SMP during a thermo-mechanical cycle

Unimorph Composite Actuator Experimental Procedures and Materials

Unimorph Composite Actuator (UCA) Fabrication

Each unimorph composite actuator consisted of a layer of SMP bonded to a CFRP substrate. Both flat CF composite unimorphs and unimorphs incorporating transverse curvature followed the same fabrication methodology. The SMP was placed on the compression side of all three actuator types so the manner of actuation was the same for each UCA configuration. A single layer of [±45°] oriented, plain weave (a one over one under pattern), bi-directional carbon fiber was cut and placed on a Teflon® covered plate or curved tooling board. The [±45°] fiber configuration was used versus a [0°/90°] because it allowed for the CF to be rolled to a smaller diameter in the stored state and was more stable during storage. The entire assembly was covered in an additional layer of Teflon®, vacuum bagged, and cured at 130 °C for 4 h. After the oven curing cycle, the carbon fiber was cut to the appropriate size, then a Veriflex-S® shape memory polymer panel was bonded to the CF using Araldite® 2011 two-part epoxy at room temperature. Once the epoxy was completely cured the composite substrate side of the actuator was coated with flat white paint. A random speckle pattern was then applied using flat black spray paint for DIC analysis later.

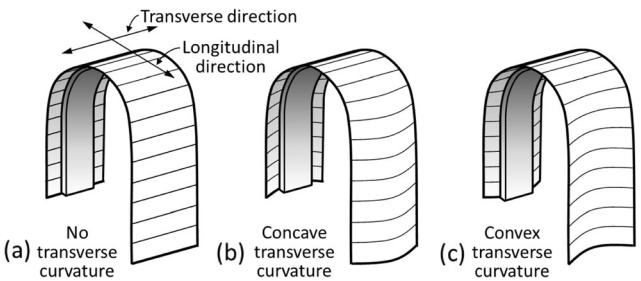

Fig. 3 Comparison of a UCA (**a**) without curvature (flat composite), (**b**) with concave transverse curvature, and (**c**) a UCA with convex transverse curvature in the stored configuration

Digital Image Correlation (DIC) Set-Ups

The primary objective of this research was to determine the deformation and shape of the actuator samples. This was done through the use of DIC, a non-contact, full-field shape and deformation measurement technique developed at the University of South Carolina [68–70]. The DIC system utilized two Point Grey Research, 5-megapixel, grayscale cameras that simultaneously captured images of the random speckle pattern applied to the samples. Images were captured via VIC-Snap™ 2009 and later processed via VIC-3D™ 2009 to determine the deformations and strains. A pair of reference images (one image per camera) of the CF substrate side of the actuators were taken after the substrate was painted and before a thermo-mechanical cycle. These reference images were contrasted against pairs of images taken over the hour observation time to determine the deflection as the sample cooled. Subsequent images were taken before starting each thermo-mechanical testing cycle. Figure 4 shows the DIC experimental set-up used to measure the residual deformation, out-of-plane position, and surface strains of the UCA specimens in the stored and deployed configurations.

Thermocouple Set-Up

A transversely curved UCA was monitored during the deployed and stored cooling stages to develop a cooling profile over time. The UCA was outfitted with two Omega® SA1 self-adhesive K-type thermocouples. A thermocouple was placed in the center of the UCA on both the top and bottom surfaces to monitor temperature.

Environmental Chamber Set-Up

The UCAs were placed in a Sun Systems® Model EC12 environmental chamber used to regulate the temperature to the desired point above the shape memory polymer glass transition temperature. The temperature was monitored via a thermocouple inside of the chamber and confirmed via a Fluke® 561 series infrared thermometer. Actuator samples were placed on a Teflon® plate within the chamber to allow for full expansion under elevated temperature conditions.

UCA Sample Holder Set-Ups

Once samples were removed from the environmental chamber after the initial 1 h soak time they were bent into a U-shaped configuration, as shown in Fig. 5(a), and stored in a tabletop retainer to ensure equivalent loading conditions for all actuators. This apparatus consisted of five 1/4-20 bolts in a U-shaped configuration secured to the table in order to constrain the samples from folding inwardly, and two metal blocks spaced 65 mm apart to constrain the samples in the outward direction. After the samples cooled in the stored configuration (Step 4 in Fig. 1) they were then placed back into the environmental chamber for another hour at 85 °C. Finally, the heated sample was placed, speckle pattern up, on the optical table to observe the residual deformation as the sample cooled (Step 7).

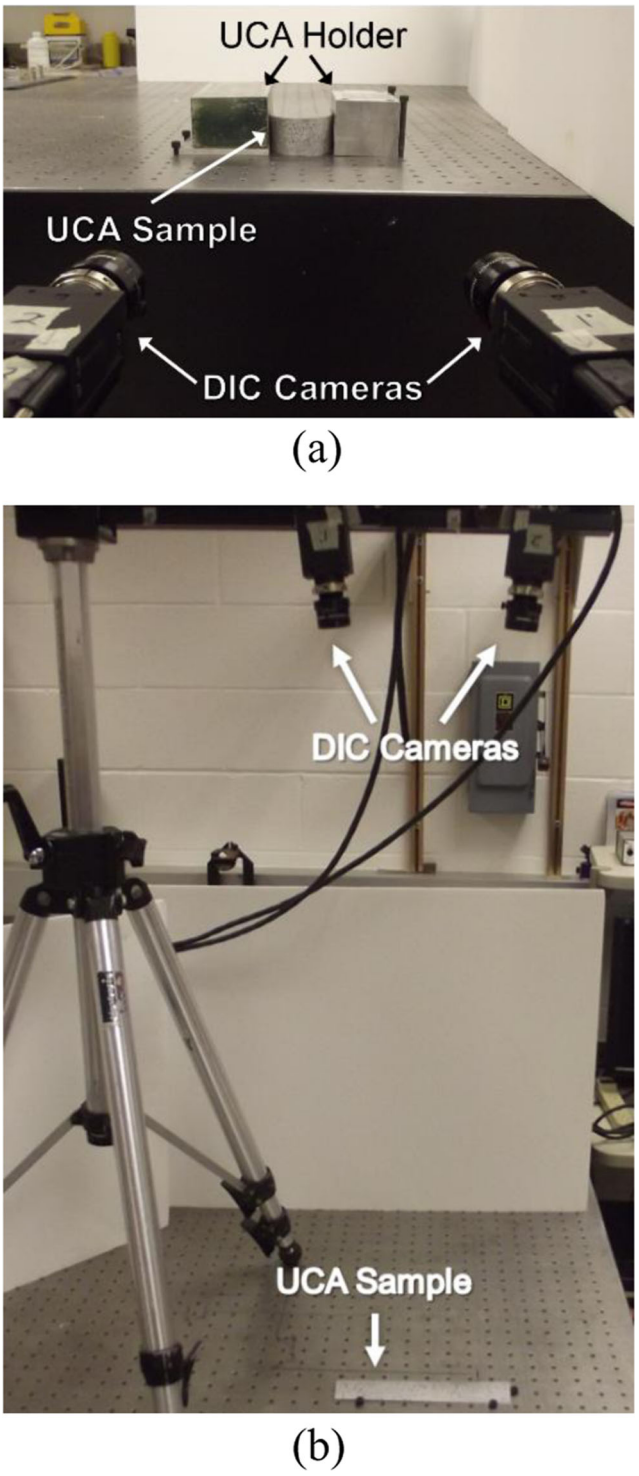

Fig. 4 Experimental set-ups for DIC analyses of the UCAs in the (**a**) stored configuration and (**b**) deployed configuration

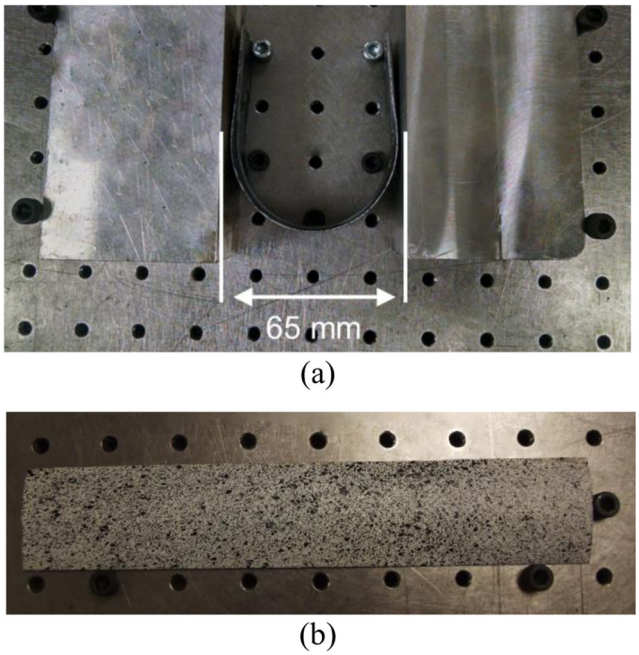

Fig. 5 The (**a**) stored sample holder constructed for housing the UCA during cooling (Step 4) and (**b**) the deployed sample registration used to ensure the UCA was in the same position after a thermo-mechanical cycle (Step 7)

Positioning, shown in Fig. 5(b), consisted of three 1/4-20 bolts placed so that the sample can be repeatedly registered with the overhead DIC cameras. This setup kept rigid body motion to a minimum, but additional post-processing ensured the removal of all rigid body motion the sample may have experienced during the thermo-mechanical cycle.

Procedure to Measure UCA Recoverability

The step-by-step procedure for measuring the out-of-plane residual deformation, surface strains, and shape recovery of the UCA using DIC after a temperature cycle is enumerated below.

Step 1. After applying a speckle pattern to the sample, take an initial (reference) image of the UCA using the DIC set-up shown in Fig. 4(b).
Step 2. Place the undeformed UCA in the environmental chamber for 1 h at 85 °C.
Step 3. Bend the UCA into a U-shaped configuration and place it within the holder to cool for 1 h in the stored configuration.
Step 4. Release the UCA from the holder and return it to the environmental chamber set to 85 °C. Allow the UCA to hold for 1 h at temperature.
Step 5. Remove UCA from the oven to start recovery to the original/programmed position shown in Fig. 5(b).
Step 6. Monitor via DIC while the UCA cools to room temperature.

Measuring the deformation in the stored configuration was completed by following steps one through three and six with the DIC cameras and sample in the configurations shown previously in Figs. 4(a) and 5(a) respectively.

Materials Characterization

In the succeeding experiments a single layer of [±45°] oriented, plain weave, bi-directional carbon fiber and a single strip of Veriflex-S® SMP were combined to create the UCAs. Before the UCAs were characterized as a unit the constituents were characterized individually. The epoxy and spray paint were not characterized due to their negligible thickness (0.15 and 0.05 mm respectively) with respect to the SMP and substrate (1.6 and 0.35 mm respectively) in the UCA. The Young's modulus and Poisson's ratio for both of these materials were calculated from a combination of tension tests and DIC to measure the full-field displacements under loading conditions at room temperature. The material properties for the CFRP were gathered with the fibers in the [±45°] orientation to coincide with the substrate lay-up. The load and corresponding strains were used to calculate the values provided in Table 1. Coefficient of thermal expansion (CTE) was determined by placing the specimens on a specialized hot plate and monitoring strain with respect to temperature via DIC similar to the technique used by both Abudarum et al. and Gdoutos et al. [71–73]. These strain values were validated by measuring the CTE of an aluminum sample concurrently with the Veriflex-S® and CFRP. Glass transition temperatures were taken from the manufacturer's respective published values. The glass transition temperature of the carbon fiber refers to the epoxy matrix's transition temperature which is well above the glass transition temperature of Veriflex® and the experimental operating temperature. Coefficient of variation (CV) which is defined as the ratio of the standard deviation to the mean is provided to display the extent of variability of the data.

Unimorph Composite Actuator Results

Initial UCA Investigation

In order to aid the reader, testing results from three UCAs with flat, convex curved, and concave curved substrates are presented to elucidate the testing procedure, analysis methods and resulting trends. A subsequent section will then cover an expanded design space to show how geometric parameters affect shape recovery. Out-of-plane deflection (w) was the main focus of the UCA experiments as it was used to determine recoverability. The goal was a UCA with minimal residual deformation after thermo-mechanical cycle(s) and that when stored would hold the desired shape. Initial samples consisted of 200 mm long by 38 mm wide flat (infinite radius

Table 1 Material properties for [±45°] oriented, plain weave, bi-directional carbon fiber and Veriflex-S® shape memory polymer

Property	CFRP [±45°]		Veriflex-S®	
	Value	CV	Value	CV
Coefficient of thermal expansion (α)	$2.5\pm0.2E^{-6}$ K^{-1}	8 %	$160\pm15E^{-6}$ K^{-1}	9.6 %
Young's modulus (E)	11.8±0.3 GPa	2.8 %	1.1±0.05 GPa	4.5 %
Poisson's ratio (ν)	0.79±0.02	2.5 %	0.39±0.01	2.6 %
Glass transition temperature[a] (T_g)	121 °C	–	62 °C	–

[a] Manufacturer published values

of curvature) and 63.5 mm radius of curvature carbon fiber substrates. The CF substrates had a thickness of 0.35 mm. A 12.7 mm wide and 1.6 mm thick strip of flat SMP adhered via a 0.15 mm thick layer of Araldite® 2011 epoxy to the center of the carbon fiber substrate. The total UCA thickness was 2.15 mm which included a 50 μm layer of paint on the substrate surface for DIC measurements. Figure 6 shows a mock-up of the key variables on a concave curved UCA. In addition to studying the out-of-plane deflection (w), experiments were conducted to determine the cooling behavior of the UCAs, the out-of-plane position (z+w) in the transverse direction, and the average strain on the UCA surface during cooling.

Post-processing of the DIC data was required to properly determine the deflection for each UCA over time. Post-processing was accomplished by extracting the xyz coordinates and uvw displacements for the centerline of each sample at the desired timestamp. Next, the data was extracted to an Excel file, the deformation (w) data sorted by timestamp, and shifted to the desired coordinate system via MATLAB. Once in the desired x-z plane, the data was rotated to eliminate rigid body motion making sure to rotate the sample in the x or lengthwise direction to maintain the correct displacement directions. After rotation the data underwent a final vertical translation to the x-axis ensuring all images can be compared in the same coordinate system. This process is illustrated in Fig. 7. The same process was used to extract and process the data for the widthwise (y-z plane) out-of-plane position (z+w) figures presented later.

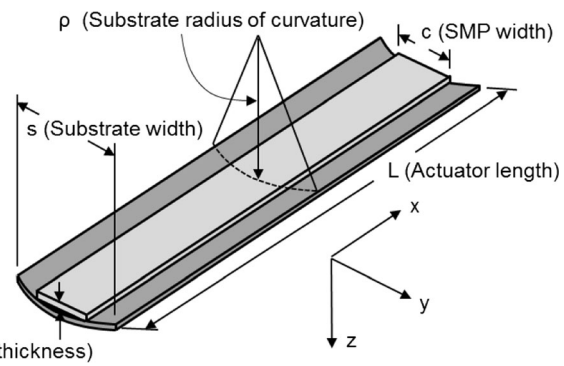

Fig. 6 Illustration of the variables of interest for this study on an original/programmed concave UCA

Data for the flat, concave, and convex UCA samples were collected in 2 min intervals for the entirety of the 30 min cool down time. The centerline shape was measured for the reference (before any temperature cycle) and at various times after the temperature cycle. To obtain the deformation (w), the reference shape was subtracted from the shape after the thermo-mechanical cycle. To obtain the out-of-plane position (z+w) the residual deformation (w) seen was added to the original undeformed shape (z) of the UCA before the thermo-mechanical cycle. In addition to the out-of-plane measurements, the strain fields were monitored in both the stored and deployed configurations, as well as thermocouple measurements on both sides of the UCA to establish a cooling profile. Repeatability and uncertainty experiments were performed during the initial experiments and expanded design space experiments respectively. These results are shown at the end of the corresponding sections to confirm the repeatability and statistical significance of the experimental results shown.

Deployed configuration results

The cooling temperature as a function of time was measured during cool down for the deployed state (Step 7). A type-K self-adhesive thermocouple was placed on the top and bottom surface to monitor the temperature as the UCA cooled. Five thermo-mechanical trials were conducted on a single UCA and the average cooling profile is shown in Fig. 8. The thermocouple measurements were accurate within ±1.5 °C and the data shows that there is no statistical difference between the top and bottom surface temperatures during cooling. The UCA cooled from 75 to 25 °C in the first 6 min, then reached ambient temperature on the surface at approximately 10 min.

Following the establishment of the deployed cooling temperature profile, experiments were conducted to determine the out-of-plane deformation (the deployed position referenced to that of the UCA before the thermo-mechanical cycle) for flat, concave, and convex UCAs. Figure 9 show the out-of-plane deflection of the centerline along the longitudinal direction for the flat, concave, and convex samples respectively through 30 min of cool down. The data clearly shows that the concave and convex samples have significantly less residual

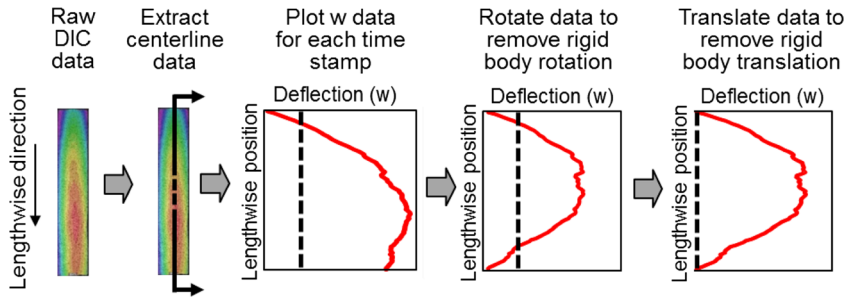

Fig. 7 Illustration of the process of converting the DIC data to the desired coordinate system and removing rigid body motion in the longitudinal direction

deformation than the flat sample over the 30 min trial. The concave sample had a maximum unrecovered deformation of only 0.35 mm while the flat sample had a maximum difference from the original shape of 12.7 mm, a nearly two order of magnitude improvement. The convex sample deflected a maximum of 1.29 mm in the same time period. The graphs show that the concave UCA reached peak deflection at approximately 6 min then relaxed a distance of 60 μm by the 30 min mark. The flat UCA continued to deflect until the 30 min mark. Lastly, the convex sample, behaved similar to the concave sample, approaching maximum deflection at 6 min and then relaxing up to the 30 min mark. The data shows that a majority of the deformation had already occurred after 6 min for all samples tested. The data matches the temperature profile results seen during the thermocouple experiments as the majority of cooling occurred in the first 6 min. After 10 min the substrate and SMP outer surfaces are at ambient temperature, however, the inner surfaces of the SMP had not reached room temperature due to the thickness differences between the substrate and SMP. The SMP continued to cool and contract from its heated state which explains the continued deflection seen in the flat UCA. The non-monotonic behavior seen in the curved UCAs is explained similarly. The carbon fiber has a CTE that is two orders of magnitude below that of the Veriflex® SMP resulting in a contraction of the SMP at a much higher rate than the carbon fiber substrate as the UCA cools. However, after both the UCA and SMP have cooled for approximately 10 min, contracting past the stability point of the UCA, the increased bending stiffness of the transversely curved substrate compensates for this mismatch in CTEs resulting in a slow relaxation to the equilibrium point. This results in a decreased residual deflection unlike the flat UCA which isn't assisted by increased bending stiffness in the substrate. The results indicate the concave curved configuration over the convex curved configuration should be used for any further testing due to the minimal deflections seen under comparable conditions.

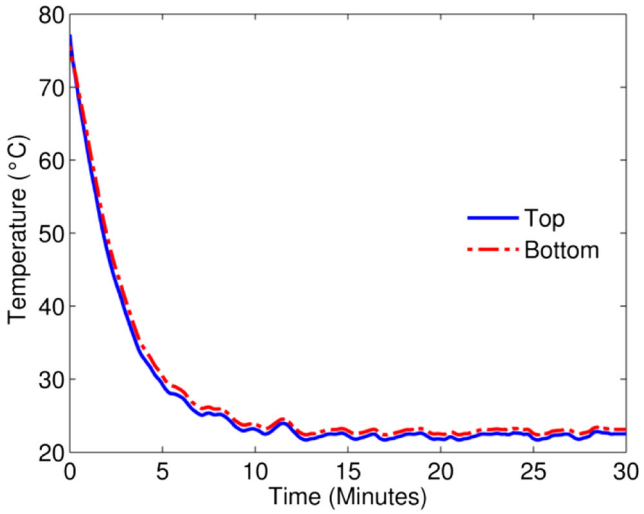

Fig. 8 The average cooling profile of five temperature cycles in the deployed configuration

The preceding tests clearly show that the concept of applying transverse curvature to a unimorph substrate substantially improved shape recovery. After determining the maximum out-of-plane deflections and their relation to transverse curvature the DIC data acquired was also used to view strain fields as the UCAs cooled. Figure 10 shows the strain fields on the flat UCA after 30 min. The strain fields were found to be fairly uniform for all samples so the center section of each UCA was selected as the area of interest, evaluated, and averaged to get an average strain value at specific times during the cooling cycle. The area of interest is exhibited in Fig. 10 as the area inside of the dashed lines. The averaged values from the area of interest are shown in Fig. 11 where it was again confirmed that a majority of the deformation occurs in the first 6 min. All of the stains at 30 min are less than approximately 0.12 % at the center of the UCA with the highest strains seen in the transverse direction of the concave UCA followed closely by flat UCA in the longitudinal direction.

The last information extracted from the DIC data for the deployed configuration was the transverse direction out-of-plane position. This data was processed in the same manner as the out-of-plane deformation, however, it was taken at the center of the UCA perpendicular to the lengthwise direction. Figure 12 displays the out-of-plane position, the original location (z) plus out-of-plane deformation (w), for each of the three UCAs. The flat UCA had almost no change in its widthwise position after a thermo-mechanical cycle while the concave UCA actually increased in transverse curvature providing greater bending stiffness than the original UCA. The concave UCA increased in height by approximately

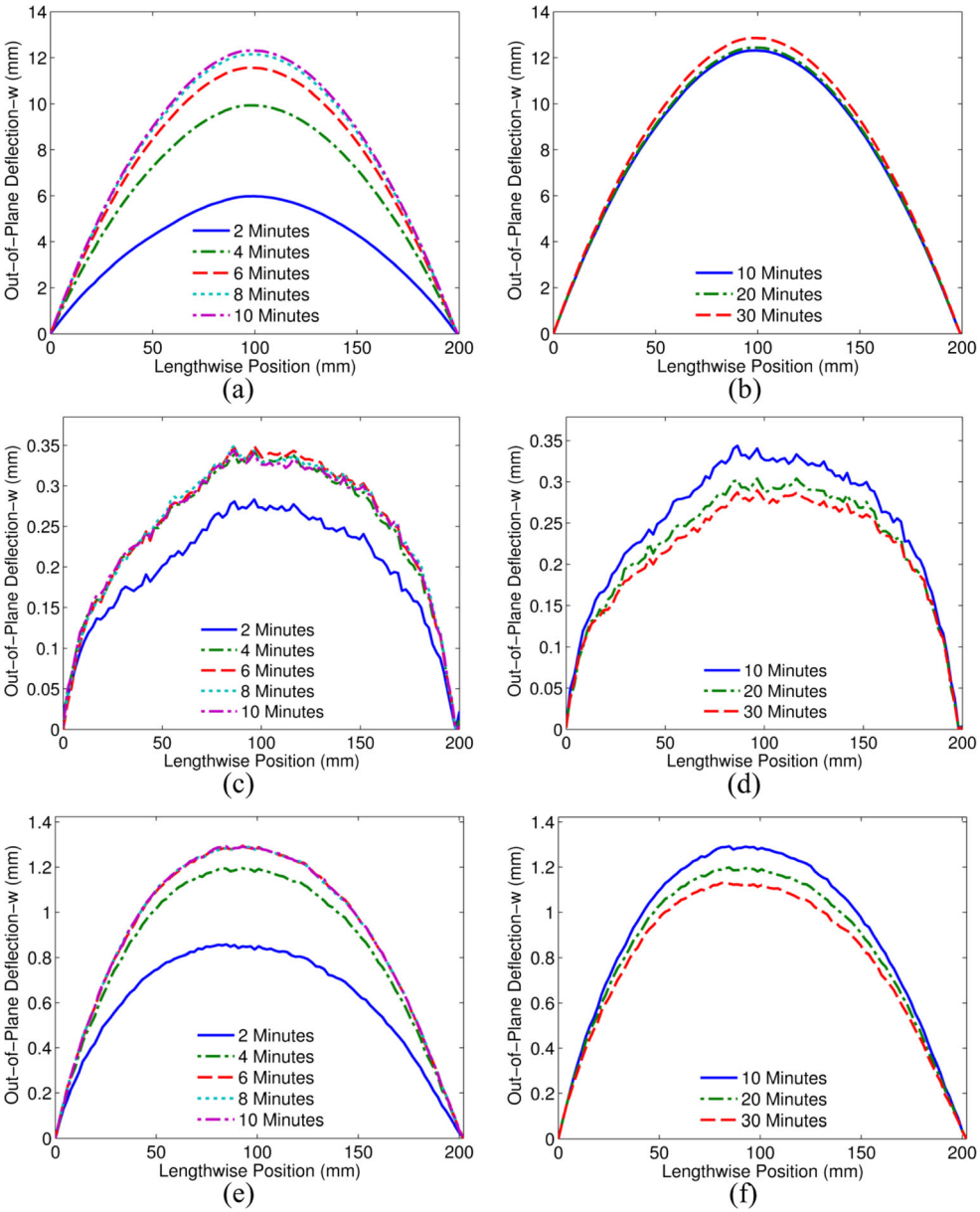

Fig. 9 Lengthwise position versus out-of-plane deflection for the (**a**) flat UCA for the first 10 min and (**b**) times 10 to 30 min of the UCA cooling cycle. The concave UCA for (**c**) the first 10 min and (**d**) times 10 to 30 min. The convex UCA for (**e**) the first 10 min and (**f**) times 10 to 30 min

0.5 mm after 30 min which is a 20 % increase in the curvature. The convex UCA actually relaxed and decreased in transverse curvature after 30 min. This decrease in transverse curvature contributed to the convex UCA performing worse than the concave UCA despite having the same initial radius of curvature.

An additional set of tests were completed on a new concave curved sample to determine the repeatability of testing and if any additional residual deformation occurred as additional thermo-mechanical cycles were performed on the UCA. A series of four consecutive tests were conducted and compared at the maximum out-of-plane position (z+w) at 6 min as well as at the end of the data collection time. Table 2 shows the data varied by only 40 μm at 6 min and 30 μm at 60 min. These values are well within an acceptable range for repeatability.

Deformed/stored configuration results

In addition to determining the characteristics of UCAs in the deployed configuration (Step 7), multiple analyses were conducted on the deformed/stored configuration (Step 4). Although the main focus of this paper is the x-direction and the out-of-plane residual deformation, for documentation and complete understanding of the thermo-mechanical cycle the strains in the stored configuration and out-of-plane deformation in the y-direction were investigated. The deformed configuration is the state in which the UCA undergoes its maximum deformation and it was crucial to determine if the UCA was still in the elastic range of deformation when stored. Ifju, et al. have shown previously that in a [±45°] configuration, carbon fiber is capable of enduring high strains with

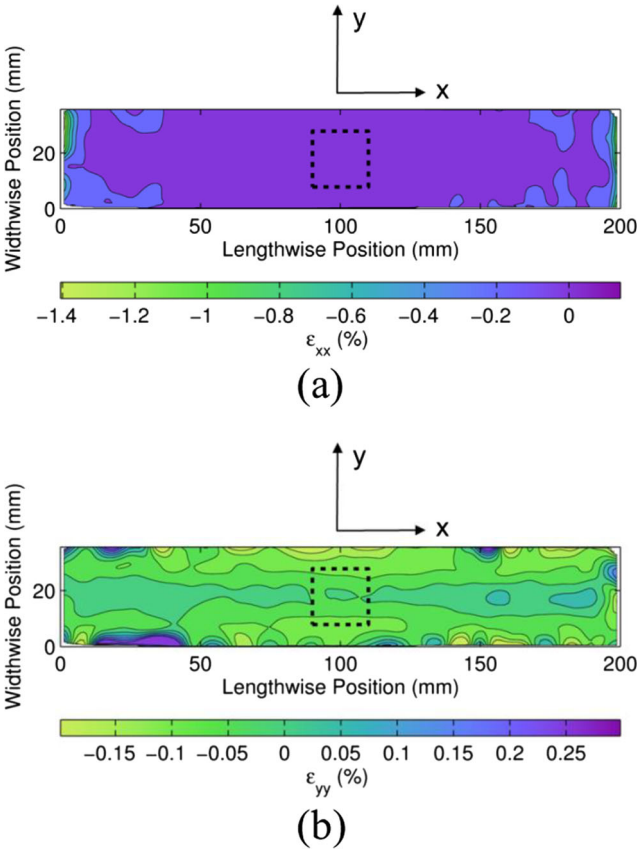

Fig. 10 The strain fields on the flat UCA in the (**a**) x-direction and (**b**) y-direction after cooling for 30 min. The area of interest for strain calculations is area enclosed by the box in the center of the specimens

minimal residual deformation when stored in a cylindrical configuration, however, it was still essential to quantify the maximum deformation and surface strains [65–67]. Similar to the original/programmed state, the cooling profile after the initial hour soak at 85 °C was established with five thermo-mechanical trials. The cooling profile closely resembled the deployed configuration profile as the UCA cools from 65 to 25 °C in the first 6 min, then reaches ambient temperature on the surface at approximately 10 min. The difference in initial

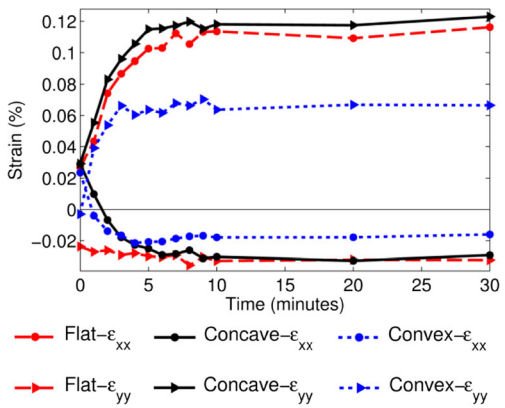

Fig. 11 Average strain at the center of the UCA during the deployed cooling cycle (Step 7) for flat, concave, and convex UCAs

cooling temperatures (75 °C for deployed vs. 65 °C for stored) is attributed to the time it took to mechanically deform the UCA after removing it from the environmental chamber for the stored configuration whereas the deployed configuration required no mechanical deformation.

After determining the cooling profile in the stored configuration the DIC data acquired in the stored configuration was evaluated for the strain fields during cooling and out-of-plane position of the three types of UCAs. Figure 13 shows the average strain on the selected surface area of the UCAs (identical to the area on the deployed UCAs) during the storage cool down. The strain fields were found to be fairly uniform with a slight decrease in the strain in the longitudinal or x-direction due to cooling during the first 6 min. Once the samples had passed this point the strains appeared to be constant until the storage cooling cycle ended. The mechanical strain from bending the UCA into the stored configuration was approximately 1 % while the thermal strain was on the order of 0.1 %. The maximum strains seen were approximately +1.15 and −0.65 % occurring in the flat UCAs x-direction and concave UCAs y-direction respectively. These strain values were determined to be still within the elastic region for [±45°] oriented carbon fiber based upon previous research.

Finally, the out-of-plane deformation in the transverse direction was extracted from the DIC data to determine the effect of transverse curvature in the stored configuration. This data was processed in the same manner as the out-of-plane deformation however, as stated previously, it was taken at the center of the UCA perpendicular to the lengthwise direction. Figure 14 displays the out-of-plane position for each of the three UCAs in the stored configuration.

All three UCAs have clearly defined reference shapes but, once placed in the storage container all have negligible transverse curvature. Each UCA had an out-of-plane position of less than 0.4 mm when in the stored position. The data shows that in the stored condition all three UCAs have nearly identical out-of-plane flattened shapes. With the knowledge gained from the evaluation of the UCAs in both the stored and deployed configurations it was determined that further investigation was needed to determine the interactions between the assorted variables in the construction of the UCAs. As a result the priority for the subsequent expanded design space investigations was limited to studying the residual deformation of the deployed UCAs due to the similarity of the UCAs deformations in the stored configuration and minimal temperature-dependent strains.

Expanded Design Space Investigation

After establishing a point of reference for the interaction between transverse curvature and residual deformation, further expansion of the design space was desired to determine the interactions between the other variables of interest and UCA

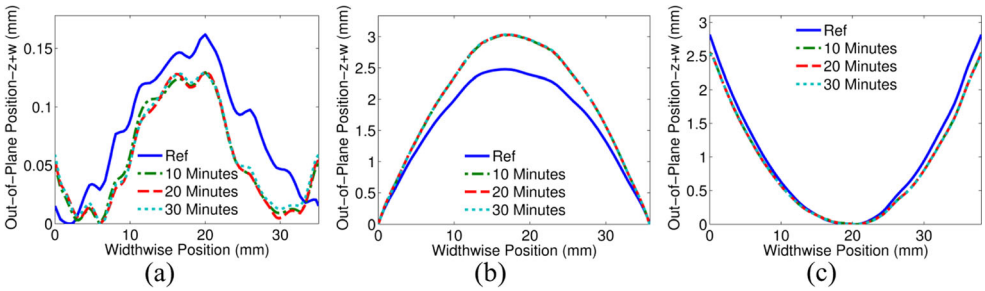

Fig. 12 The widthwise position versus out-of-plane position (z+w) for the reference and 10 to 30 min into the cooling cycle for the (**a**) flat, (**b**) concave, and (**c**) convex UCAs in the deployed position

residual deformation. Only the concave curved UCA was tested and compared to the baseline flat UCA in the expanded design space because the convex curved UCA performed an order of magnitude worse than the concave UCA despite having the same amount of transverse curvature. As illustrated previously in Fig. 6 there were five variables of significance: actuator length, substrate radius of curvature, substrate width, SMP width, and SMP thickness. Two of the variables were eliminated from the investigation as fixing the SMP width and actuator length was required to conserve material as a limited amount of shape memory material was available. Eliminating these variables left substrate radius of curvature, SMP thickness, and substrate width as the three variables that would be altered during the expanded design space investigation. Three transverse curvatures were investigated and given the succeeding designations; **flat** (infinite radius of curvature), **low transverse curvature** (127 mm radius of curvature), and **high transverse curvature** (63.5 mm radius of curvature). Two SMP thicknesses were investigated; **thin** (0.8 mm) and **thick** (1.6 mm). Finally, three substrate widths were tested; **narrow** (25.4 mm), **intermediate** (38.1 mm), and **wide** (50.8 mm). This led to a total of 18 different combinations of UCAs. Table 3 shows the different curvatures, thicknesses, and widths chosen for investigation and their respective designations.

Once all samples were tested for a minimum of three thermo-mechanical cycles the data was analyzed and the maximum out-of-plane deflection was calculated for each UCA. The data is shown below in Fig. 15 for the 18 samples investigated. The flat and high transverse curvature samples with thick SMP and intermediate substrate width, were identical to the flat and concave samples tested previously.

Table 2 Repeatability testing data for the concave UCA sample

Time	6 min	60 min
Trial 1 positions	1.93 mm	1.81 mm
Trial 2 positions	1.95 mm	1.80 mm
Trial 3 positions	1.91 mm	1.78 mm
Trial 4 positions	1.93 mm	1.81 mm
St. dev.	16 μm	14 μm
CV	0.85 %	0.78 %

Upon analyzing the data, clear trends emerged in changing transverse curvature, SMP thickness, and substrate width. As the UCA's transverse curvature increased, the amount of residual deformation decreased dramatically. The larger the transverse curvature (or smaller radius of curvature) of the substrate, the greater the observed recoverability (or lack of permanent deformation). The out-of-plane deflection decreased from 27.7 mm for the flat, intermediate width, thin SMP samples to 0.34 and 0.26 mm for the low and high curvature samples respectively. This demonstrated a two order of magnitude improvement as a result of including transverse curvature in the substrate of a UCA. As SMP thickness increased residual deformation also increased in samples with transverse curvature. The opposite trend was seen in the flat UCAs. Additionally, deformation decreased considerably as the carbon fiber width increased from a narrow to intermediate width. Increasing from the intermediate to wide CF width did not have a tendency to decrease the deformation as markedly as the previous increase in width. In some cases increasing the CF substrate width actually increased deflection. The trend of maximum deflection versus carbon fiber width is shown in Fig. 16 for high transverse curvature UCAs made with thick SMP. In general, a wider composite substrate modestly aided recoverability with diminishing returns.

When progressing from the stored state (Step 4) to the deployed state (Step 7), the carbon fiber will achieve an equilibrium point where the transverse curvature in the widthwise

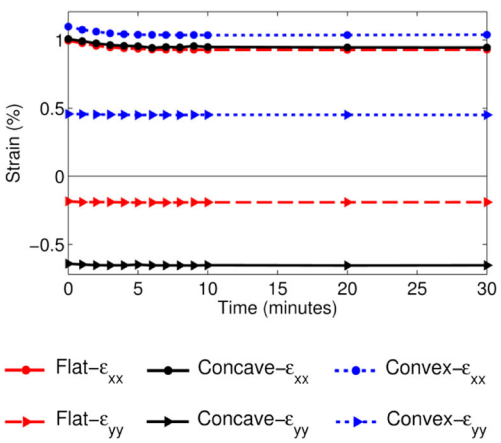

Fig. 13 Average strain at the center of the UCAs during the deformed/stored cooling cycle (Step 4) for the three UCA types

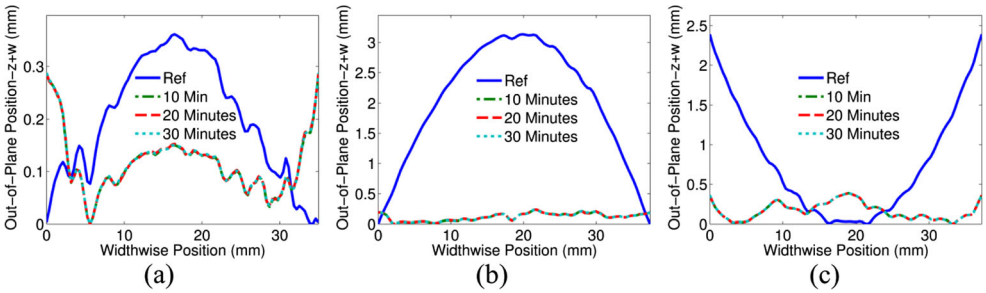

Fig. 14 The widthwise position versus out-of-plane position (z+w) for the reference and 10 to 30 min into the cooling cycle for the (**a**) flat, (**b**), concave, and (**c**) convex UCAs in the stored position

direction is nearly flat. Most samples can easily snap through this middle state due to the transverse curvature in the substrate and return to the deployed shape. However, for the low transverse curvature sample with thick SMP and a wide substrate this point acted as an unstable equilibrium point between two stable equilibria and thus resulted in elevated residual deformation compared to that seen in the other UCA sets. This equilibrium point was also seen in the flat sample with thick SMP and wide substrate as the residual deformation was nearly identical due to the combination of CF width and lack of transverse curvature. This is illustrated in Fig. 17 which shows the out-of-plane position (z+w) of the reference transverse curvature versus the curvature after a thermo-mechanical cycle. The graphs show that the flat, wide substrate, thick SMP UCA and the low transverse curvature, wide substrate, thick SMP UCA had similar maximum out-of-plane positions in the transverse direction and out-of-plane deformation in the longitudinal direction after a thermo-mechanical cycle. These findings further established that this is an unstable equilibrium point between the stored and deployed states of the UCA.

Analysis of the samples with respect to curvature provides confirmation that an increase in curvature does significantly reduce residual deflection and allow greater recovery of the UCA. The flat sample with thin SMP and intermediate substrate has a maximum deflection of 27.7 mm while increasing to the highest transverse curvature decreases maximum curvature to 0.26 mm. This is a reduction of deflection of two orders of magnitude by adding a minute amount of transverse curvature to the UCA. The trend of maximum deflection versus increasing transverse curvature is shown in Fig. 18 holding SMP thickness and CF width constant. These findings display definitive evidence that an increase in transverse curvature allows for greater recovery of the UCA and reduces residual deflection in the samples.

In order to verify the expanded design space results a series of tests were completed to quantify the uncertainty and determine if the results were statistically significant. Due to limited material availability only eight flat, thin SMP, intermediate substrate width samples and eight high transverse curvature, thin SMP, intermediate substrate width samples were tested to

Table 3 Radius of curvature (ρ), SMP thickness (t), and substrate width (s) possibilities and their respective designations for the UCAs investigated

Nomenclature and supporting values			
Transverse curvature	Flat	Low	High
Radius of curvature (ρ)	∞	127 mm	63.5 mm
SMP thickness (t)	Thin	Thick	–
Thickness values	0.8 mm	1.6 mm	
Substrate width (s)	Narrow	Intermediate	Wide
Width values	25.4 mm	38.1 mm	50.8 mm

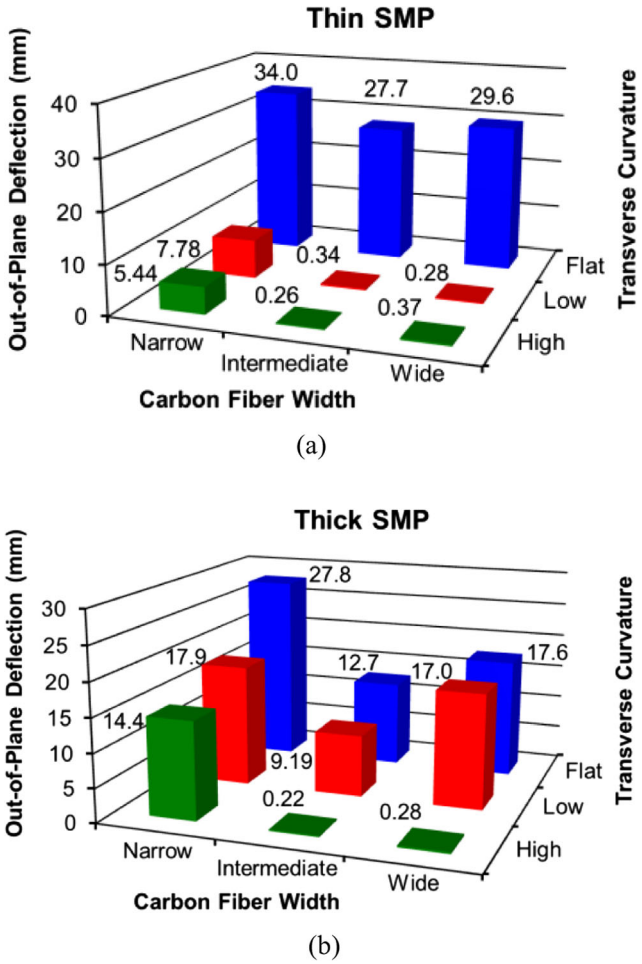

Fig. 15 Maximum out-of-plane deflection at the end of the 60 min observation period for the deployed state keeping thickness constant for the (**a**) thin SMP and (**b**) thick SMP UCAs

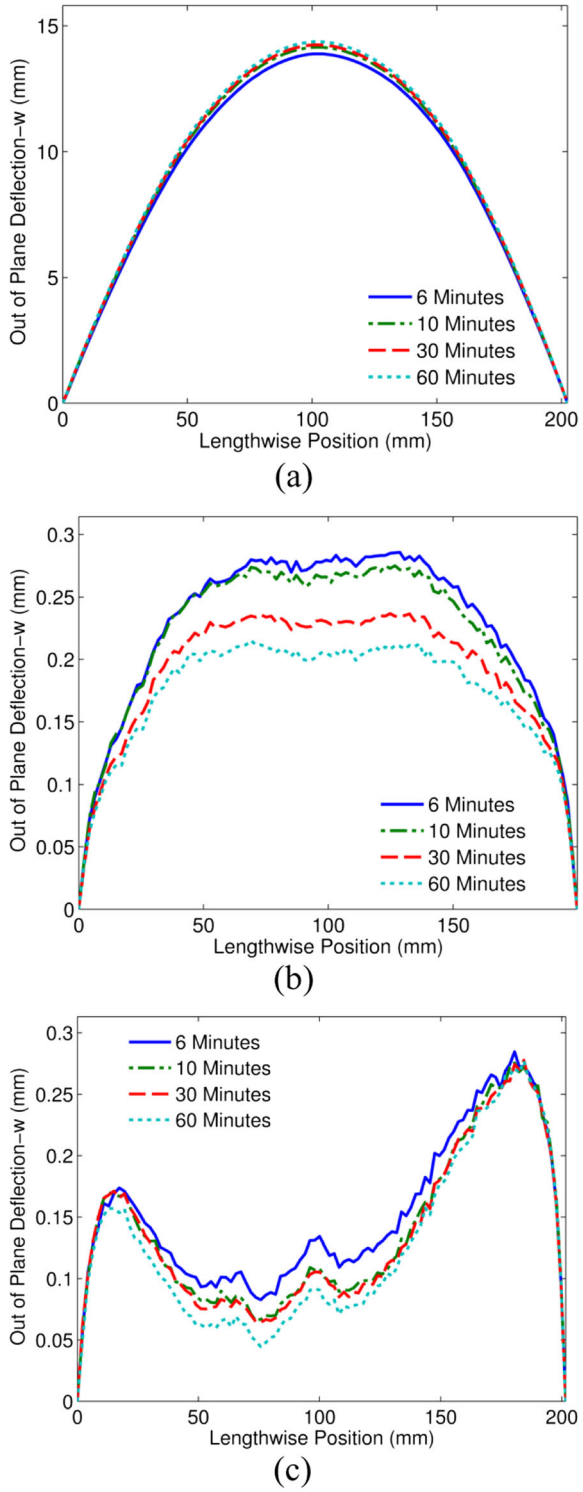

Fig. 16 Lengthwise position versus out-of-plane deflection for the high transverse curvature, thick SMP, (**a**) narrow, (**b**) intermediate, and (**c**) wide substrate UCA cooling cycles

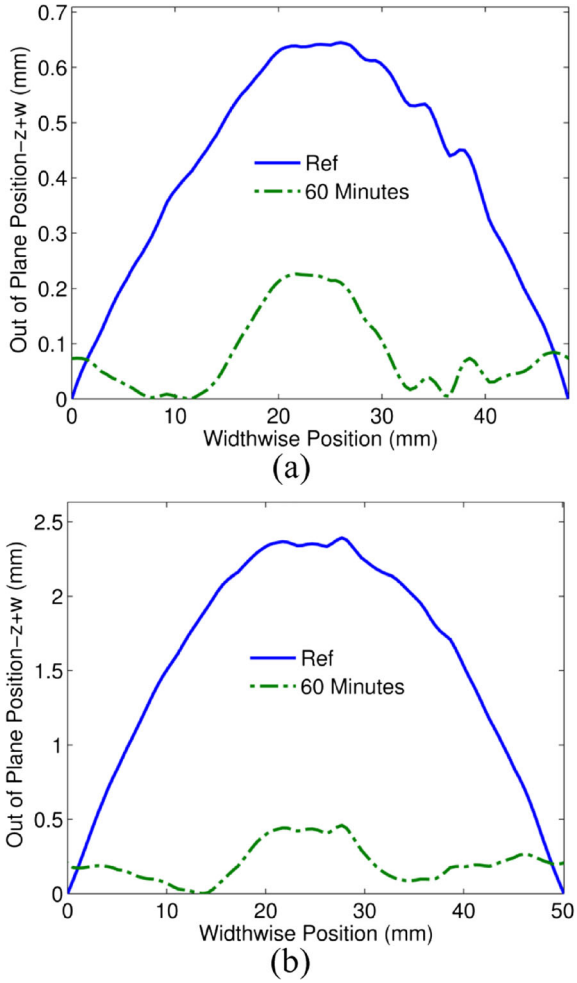

Fig. 17 Widthwise position versus out-of-plane position for the thick SMP, wide substrate UCAs with (**a**) flat curvature and (**b**) low transverse curvature

determine the out-of-plane deflection range for the UCAs. These two variants were selected as determining the statistical significance of curvature was the first priority. Each sample was evaluated using the same methodology established earlier and the centerline data extracted for examination. Figure 19 shows the eight out-of-plane deflections for both samples at the 60 min mark.

These tests show that the maximum standard deviation for the flat, thin SMP, intermediate substrate width sample was ±2.2 mm with an average maximum out-of-plane deflection of 26 mm. The maximum standard deviation for high transverse curvature, thin SMP, intermediate substrate width sample was ±0.1 mm with an average maximum out-of-plane deflection of 0.26 mm. In addition to testing the high radius of curvature and flat UCAs, a single [±45°] layer of intermediate width carbon fiber of each radius of curvature underwent a thermo-mechanical cycle. The purpose was to determine the out-of-plane deflection of just the CF component to the UCA and find its contribution to the total UCA deflection. After running tests on all three radii with intermediate widths the out-of-plane deflections were 0.20 mm for the high, 0.80 mm for

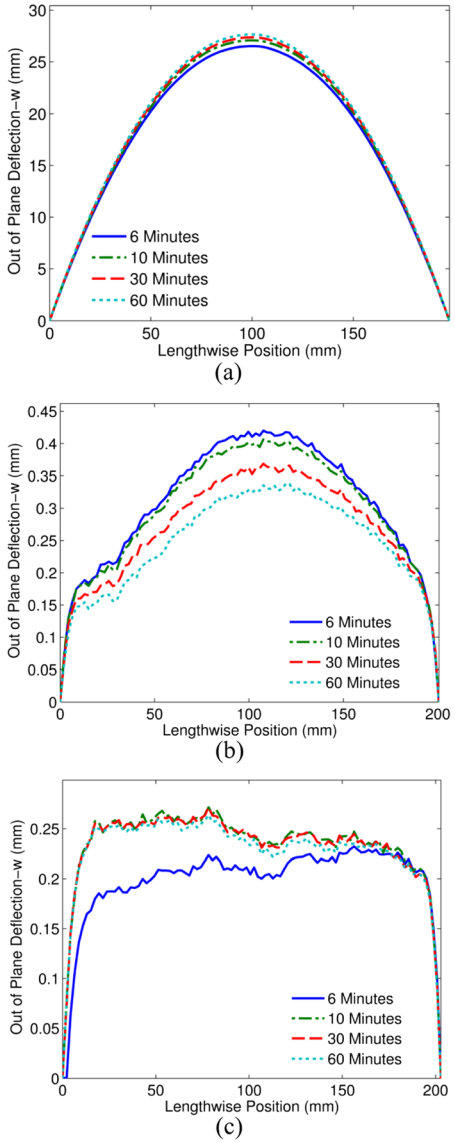

Fig. 18 Lengthwise position versus out-of-plane deflection for the (**a**) flat, (**b**) low transverse curvature and (**c**) high transverse curvature, thin SMP, intermediate substrate width UCA cooling cycles

the low, and 0.89 mm for the flat transverse curvature. The out-of-plane deflections for flat and high transverse curvature samples are on the same order of magnitude as the standard deviations presented previously. Thus, it can be concluded that the carbon fiber alone is not a significant factor in the differences in out-of-plane deflections of the flat and high transverse curvature samples. These tests prove a statistically significant difference in the out-of-plane deflection as transverse curvature increases. Extrapolating this data to other test cases indicates that changes in carbon fiber width, shape memory polymer thickness, and carbon fiber radius of curvature must be evaluated on a case-by-case basis to determine if there is a statistical difference.

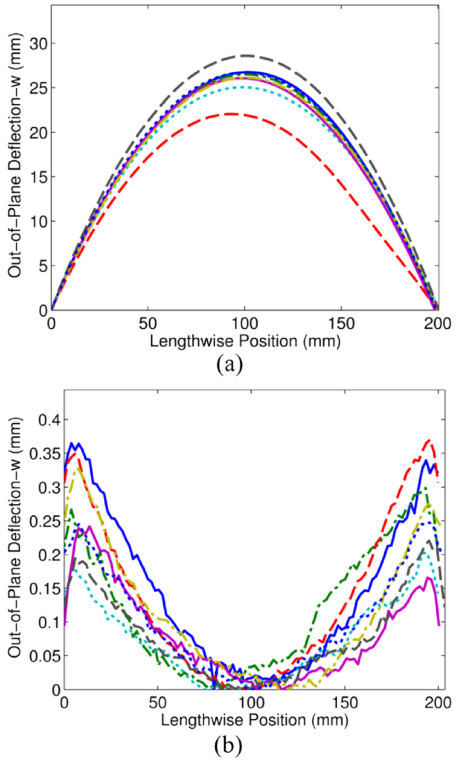

Fig. 19 Out-of-plane deflection for eight (**a**) flat, thin SMP, intermediate substrate width samples and for eight (**b**) high transverse curvature, thin SMP, intermediate substrate width samples

Conclusion

A series of tests were conducted on carbon-fiber-reinforced-polymer and shape memory polymer composite actuators to determine the effect of radius of curvature on the residual deformation. Digital image correlation was employed to measure the out-of-plane deformation and allowed for the study of the recovery behavior of these unimorph composite actuators. In the experiments conducted, a unimorph composite actuator with a 63.5 mm radius of curvature was able to reduce residual deformation by two orders of magnitude compared to a flat unimorph composite actuator keeping all other variables constant. Increased transverse curvature resulted in decreased deformation regardless of other variables. Increasing the carbon fiber substrate width of the unimorph composite actuators had a measureable effect. The less pronounced results of increasing from 38.1 to 50.8 mm suggest diminishing returns with increasing substrate width. In general, reducing shape memory polymer thickness lessened out-of-plane residual deformation, the exception being when it was adhered to a flat substrate. Unimorph composite actuators display repeatable actuation and storage cycles as they do not increase residual deformation with increasing number of cycles. These discoveries can facilitate the expanded use of shape memory polymers on reconfigurable, folding wing micro air vehicles as well as various other applications.

References

1. Nettles D (2009) Thermomechanical characterization of a shape memory polymer based syntactic foam. 1–83
2. Li G, Nettles D (2010) Thermomechanical characterization of a shape memory polymer based self-repairing syntactic foam. Polymer (Guildf) 51:755–762. doi:10.1016/j.polymer.2009.12.002
3. Volk BL (2009) Thermomechanical characterization amd modeling of shape memory polymers. 124
4. Liang F, Sivilli R, Gou J et al (2013) Electrical actuation and shape recovery control of shape-memory polymer nanocomposites. Int J Smart Nano Mater 4:167–178. doi:10.1080/19475411.2013.837846
5. Lu H, Liang F, Gou J (2011) Nanopaper enabled shape-memory nanocomposite with vertically aligned nickel nanostrand: controlled synthesis and electrical actuation. Soft Matter 7:7416–7423. doi:10.1039/c1sm05765k
6. Lu H, Gou J, Leng J, Du S (2011) Magnetically aligned carbon nanotube in nanopaper enabled shape-memory nanocomposite for high speed electrical actuation. Appl Phys Lett 98:174105. doi:10.1063/1.3585669
7. Yu X, Zhou S, Zheng X et al (2009) A biodegradable shape-memory nanocomposite with excellent magnetism sensitivity. Nanotechnology 20:235702. doi:10.1088/0957-4484/20/23/235702
8. Schmidt AM (2006) Electromagnetic activation of shape memory polymer networks containing magnetic nanoparticles. Macromol Rapid Commun 27:1168–1172. doi:10.1002/marc.200600225
9. Razzaq MY, Anhalt M, Frormann L, Weidenfeller B (2007) Mechanical spectroscopy of magnetite filled polyurethane shape memory polymers. Mater Sci Eng A 471:57–62. doi:10.1016/j.msea.2007.03.059
10. Beblo R V. (2010) Characterization and modeling of light activated shape memory polymer. 218
11. Lendlein A, Jiang H, Junger O, Langer R (2005) Light-induced shape-memory polymers. Nature 434:695–697. doi:10.1038/nature03438.1
12. Leng J, Zhang D, Liu Y et al (2010) Study on the activation of styrene-based shape memory polymer by medium-infrared laser light. Appl Phys Lett 96:111905. doi:10.1063/1.3353970
13. Vaia R (2005) Remote-controlled actuators. Nature 4:429–430
14. Maitland DJ, Metzger MF, Schumann D et al (2002) Photothermal properties of shape memory polymer micro-actuators for treating stroke. Lasers Surg Med 30:1–11. doi:10.1002/lsm.10007
15. Otsuka K, Wayman CM (1998) Shape memory materials, 1st ed. 284
16. LaCroix BW, Ifju PG (2012) Utilization and performance enhancements of multiple piezoelectric actuators on micro air vehicles. AIAA Aerosp. Sci. Meet. American Institute of Aeronautics and Astronautics, Nashville, pp 1–14
17. Lacroix BW, Ifju PG (2013) Macro fiber composites and substrate materials for MAV Wing Morphing. Soc. Exp. Mech. Society of Experimental Mechanics, Lombard, pp 1–13
18. Yakacki CM, Shandas R, Lanning C et al (2007) Unconstrained recovery characterization of shape-memory polymer networks for cardiovascular applications. Biomaterials 28:2255–2263. doi:10.1016/j.biomaterials.2007.01.030
19. Thill C, Etches J, Bond I, et al (2008) Morphing skins. Aeronaut J 1–23
20. Gross KE (2008) Mechanical characterization of shape memory polymers to assess candidacy as morphing aircraft skin. University of Pittsburgh
21. Yin W, Liu J, Leng J (2009) Deformation analysis of shape memory polymer for morphing wing skin under airflow. Front Mech Eng Chin 4:447–449. doi:10.1007/s11465-009-0062-5
22. Joo J, Smyers B, Beblo R et al (2011) Load-bearing multi-functional structure with direct thermal harvesting for thermally activated reconfigurable wing design. Int. Conf. Compos. Mater. Society of Composite Materals, Jeju, pp 1–6
23. Ko S-H, Bae J-S, Rho J-H (2014) Development of a morphing flap using shape memory alloy actuators: the aerodynamic characteristics of a morphing flap. Smart Mater Struct 23:074015. doi:10.1088/0964-1726/23/7/074015
24. Rauscher SG (2008) Testing and analysis of shape-memory polymers for morphing aircraft skin application by by. 160
25. Li G, Asce M, Xu T (2011) Thermomechanical characterization of shape memory polymer – based self-healing syntactic foam sealant for expansion joints. J Transp Eng 805–814. doi: 10.1061/(ASCE)TE.1943-5436.0000279
26. Nji J, Li G (2010) A biomimic shape memory polymer based self-healing particulate composite. Polymer (Guildf) 51:6021–6029. doi:10.1016/j.polymer.2010.10.021
27. Li G, John M (2008) A self-healing smart syntactic foam under multiple impacts. Compos Sci Technol 68:3337–3343. doi:10.1016/j.compscitech.2008.09.009
28. Fulcher JT, Karaca HE, Tandon GP, Lu YC (2012) Thermomechanical and shape memory properties of thermosetting shape memory polymer under compressive loadings. J Appl Polym Sci. doi:10.1002/app.38791
29. Fulcher JT (2011) Mechanical characterizations of environmentally conditioned shape memory polymers for reconfigurable aerospace structures. 65
30. Fulcher JT, Karaca HE, Tandon GP et al (2011) Multiscale characterization of water-,oil-,and uv-conditioned shape-memory polymer under compression. In: Proulx T (ed) Mechanics of time-dependent materials and processes in conventional and multifunctional materials. Society of Experimental Mechanics, Uncasville, pp 97–103
31. Fulcher JT, Lu YC, Tandon GP, Foster DC (2010) Thermomechanical characterization of shape memory polymers using high temperature nanoindentation. Polym Test 29:544–552. doi:10.1016/j.polymertesting.2010.02.001
32. Nahid MNH, Wahab MAA, Lian K (2011) Degradation of shape memory polymer due to water and diesel fuels. In: Proulx T (ed) Mechanics of time-dependent materials and processes in conventional and multifunctional materials. Society of Experimental Mechanics, Uncasville, pp 37–48
33. McClung AJW, Tandon GP, Goecke KE, Baur JW (2011) Non-contact technique for characterizing full-field surface deformation of shape memory polymers at elevated and room temperatures. Polym Test 30:140–149. doi:10.1016/j.polymertesting.2010.11.010
34. McClung AJW, Ruggles-Wrenn MB (2009) Strain rate dependence and short-term relaxation behavior of a thermoset polymer at elevated temperature: experiment and modeling. J Press Vessel Technol 131:031405. doi:10.1115/1.3110025
35. McClung AJW, Tandon GP, Baur JW (2011) Fatigue cycling of shape memory polymer resin. In: Proulx T (ed) Mechanics of time-dependent materials and processes in conventional and multifunctional materials. Springer New York, New York, pp 119–127
36. McClung AJW, Tandon GP, Baur JW (2011) Strain rate- and temperature-dependent tensile properties of an epoxy-based, thermosetting, shape memory polymer (Veriflex-E). Mech Time-Dependent Mater 16:205–221. doi:10.1007/s11043-011-9148-7
37. McClung AJW, Tandon GP, Baur JW (2011) Deformation rate-, hold time-, and cycle-dependent shape-memory performance of Veriflex-E resin. Mech Time-Dependent Mater 17:39–52. doi:10.1007/s11043-011-9157-6
38. Yu K, McClung AJW, Tandon GP et al (2014) A thermomechanical constitutive model for an epoxy based shape memory polymer and its parameter identifications. Mech Time-Dependent Mater 18:453–474. doi:10.1007/s11043-014-9237-5

39. Lu H (2013) State diagram of phase transition temperatures and solvent-induced recovery behavior of shape-memory polymer. J Appl Polym Sci 127:2896–2904. doi:10.1002/app.37683
40. Lu H, Liu Y, Gou J et al (2011) Surface coating of multi-walled carbon nanotube nanopaper on shape-memory polymer for multifunctionalization. Compos Sci Technol 71:1427–1434. doi:10.1016/j.compscitech.2011.05.016
41. Lu H, Yu K, Liu Y, Leng J (2010) Sensing and actuating capabilities of a shape memory polymer composite integrated with hybrid filler. Smart Mater Struct 19:065014. doi:10.1088/0964-1726/19/6/065014
42. Lu H, Liu Y, Leng J, Du S (2010) Qualitative separation of the physical swelling effect on the recovery behavior of shape memory polymer. Eur Polym J 46:1908–1914. doi:10.1016/j.eurpolymj.2010.06.013
43. Chowdhury AMS, Schmidt C, Neuking K, Eggeler G (2013) Comparative studies on the accumulation of strain and recovery ratio of Veriflex(R), a shape-memory polymer for a high strain (isin m = 210 %): Atomic force microscopic experiments. High Perform Polym 26:20–26. doi:10.1177/0954008313494907
44. Chowdhury AMS, Schmidt C, Neuking K, Eggeler G (2013) Comparative studies on the accumulation of strain and recovery ratio of Veriflex(R), a shape-memory polymer: infrared and laser experiments. High Perform Polym 25:886–893. doi:10.1177/0954008313487929
45. Liu Y, Gall K, Dunn ML et al (2006) Thermomechanics of shape memory polymers: Uniaxial experiments and constitutive modeling. Int J Plast 22:279–313. doi:10.1016/j.ijplas.2005.03.004
46. Cortes P, Terzak J, Kubas G et al (2014) The morphing properties of a vascular shape memory composite. Smart Mater Struct 23:015018. doi:10.1088/0964-1726/23/1/015018
47. Beblo R, Gross K, Mauck Weiland L (2010) Mechanical and curing properties of a styrene-based shape memory polymer. J Intell Mater Syst Struct 21:677–683. doi:10.1177/1045389X10364860
48. Beblo R, Weiland LM (2008) Strain induced anisotropic properties of shape memory polymer. Smart Mater Struct 17:055021. doi:10.1088/0964-1726/17/5/055021
49. Atli B, Gandhi F, Karst G (2008) Thermomechanical characterization of shape memory polymers. J Intell Mater Syst Struct 20:87–95. doi:10.1177/1045389X07086689
50. Carrell J, Tate D, Wang S, Zhang H-C (2011) Shape memory polymer snap-fits for active disassembly. J Clean Prod 19:2066–2074. doi:10.1016/j.jclepro.2011.06.027
51. Lan X, Liu Y, Lv H et al (2009) Fiber reinforced shape-memory polymer composite and its application in a deployable hinge. Smart Mater Struct 18:024002. doi:10.1088/0964-1726/18/2/024002
52. Leng J, Lu H, Liu Y, et al (2009) Shape-memory polymers — a class of novel smart materials. 34
53. Voit W, Ware T, Dasari RR et al (2010) High-strain shape-memory polymers. Adv Funct Mater 20:162–171. doi:10.1002/adfm.200901409
54. Monkman G (2000) Advances in shape memory polymer actuation. Mechatronics 10:489–498. doi:10.1016/S0957-4158(99)00068-9
55. Schmidt C, Neuking K, Eggeler G (2008) Functional fatigue of shape memory polymers. Adv Eng Mater 10:922–927. doi:10.1002/adem.200800213
56. Gall K, Mikulas M, Munshi NA et al (2000) Carbon fiber reinforced shape memory polymer composites. J Intell Mater Syst Struct 11:877–886. doi:10.1106/EJGR-EWNM-6CLX-3X2M
57. Beloshenko VA, Varyukhin VN, Voznyak YV (2005) The shape memory effect in polymers. Russ Chem Rev 74:265–283. doi:10.1070/RC2005v074n03ABEH000876
58. Liu C, Qin H, Mather PT (2007) Review of progress in shape-memory polymers. J Mater Chem 17:1543. doi:10.1039/b615954k
59. Vaia R, Baur J (2008) Materials science: adaptive composites. Science 319:420–421. doi:10.1126/science.1152931
60. Cantrell JT, LaCroix BW, Ifju PG (2013) Passive roll compensation on micro air vehicles with perimeter reinforced membrane wings. 51st AIAA Aerosp. Sci. Meet. American Institute of Aeronautics and Astronautics, Grapevine, Texas, pp 1–12
61. Ifju PG, Jenkins DA, Waszak MR, et al (2002) Flexible-wing-based micro air vehicles. J Am Inst Aeronaut Astronaut 1–13
62. Shyy W, Ifju P, Viieru D (2005) Membrane wing-based micro air vehicles. Appl Mech Rev 58:283. doi:10.1115/1.1946067
63. Stanford B, Ifju P (2008) Aeroelastic topology optimization of membrane structures for micro air vehicles. Struct Multidiscip Optim 38:301–316. doi:10.1007/s00158-008-0292-x
64. Albertani RJ, Stanford B, DeLoach R et al (2008) Wind-tunnel testing and modeling of a micro air vehicle with flexible wings. J Aircr 45:1025–1032. doi:10.2514/1.33338
65. Ifju P, Lee K, Albertani R et al (2008) Bendable wing for micro air vehicle. 2:11
66. Jagdale V, Stanford B, Claxton D et al (2006) Experimental characterization of load stiffening wing for small UAV. Soc Exp Mech 1–7
67. Johnson B, Claxton D, Stanford B, et al (2006) Development of a composite bendable-wing micro air vehicle. J Am Inst Aeronaut Astronaut 1–16
68. Sutton MA, Turner JL, Bruck HA, Chae TA (1991) Full-field representation of discretely sampled surface deformation for displacement and strain analysis. Exp Mech 31:168–177
69. Sutton MA (2008) Springer handbook of experimental solid mechanics. 565–600
70. Sutton MA, Orteu JJ, Schreier H (2009) Image correlation for shape, motion and deformation measurements: basic concepts, theory and applications. 342
71. Abudaram YJ, Ifju PG, Hubner JP, Ukeiley L (2013) Controlling pretension of silicone membranes on micro air vehicle wings. J Strain Anal Eng Des 49:161–170. doi:10.1177/0309324713490926
72. Yamamoto N, Gdoutos E, Toda R et al (2014) Thin films with ultra-low thermal expansion. Adv Mater 26:3076–3080. doi:10.1002/adma.201304997
73. Gdoutos E, Shapiro AA, Daraio C (2013) Thin and thermally stable periodic metastructures. Exp Mech 53:1735–1742. doi:10.1007/s11340-013-9748-z